

Hybrid Magnetic Superconductors Formed by TaS₂ Layers and Spin Crossover Complexes

Eugenio Coronado,^{*,†} Mónica Giménez-Marqués,[†] Carlos Martí-Gastaldo,^{†,§} Guillermo Mínguez Espallargas,[†] Efrén Navarro-Moratalla,[†] and João C. Waerenborgh[‡]

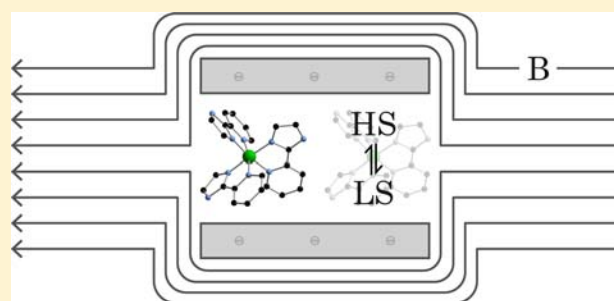
[†]Instituto de Ciencia Molecular (ICMol), Universidad de Valencia, Catedrático José Beltrán Martínez no. 2, 46980 Paterna, Spain

[‡]Dept. Química, IST/ITN, Instituto Superior Técnico, Universidade Técnica de Lisboa, CFMC-UL, 2686-953 Sacavém, Portugal

[§]Department of Chemistry, University of Liverpool, Crown Street, L697ZD Liverpool, United Kingdom

S Supporting Information

ABSTRACT: The restacking of charged TaS₂ nanosheets with molecular counterparts has so far allowed for the combination of superconductivity with a manifold of other molecule-intrinsic properties. Yet, a hybrid compound that blends superconductivity with spin crossover switching has still not been reported. Here we continue to exploit the solid-state/molecule-based hybrid approach for the synthesis of a layered TaS₂-based material that hosts Fe²⁺ complexes with a spin switching behavior. The chemical design and synthetic aspects of the exfoliation/restacking approach are discussed, highlighting how the material can be conveniently obtained in the form of highly oriented easy-to-handle flakes. Finally, proof of the presence of both phenomena is provided by the use of a variety of physical characterization techniques. The likely sensitivity of the intercalated Fe²⁺ complexes to external stimuli such as light opens the door for the study of synergistic effects between the superconductivity and the spin crossover switching at low temperatures.



INTRODUCTION

The chemical design of new materials in which distinct physical properties are brought into a single solid phase continues attracting attention within the field of materials chemistry.¹ The molecular building-block approach, which consists in the combination of different molecular functional entities, is just one example of a variety of different methods that are nowadays employed to tackle the synthesis of hybrid multifunctional materials.² An alternative tactic that is currently drawing interest is that relying on the combination of molecule-based materials with solid-state hosts. Via direct intercalation, the methodology has allowed for the controlled assembly of functional molecules into mesoporous frameworks.³ More recently, it has also permitted us to confine the growth of cyanide-bridged molecular magnets in two-dimensions.⁴

However, the direct ionic exchange procedures used in the latter reports present some drawbacks in the design of more complex hybrid materials. Indeed, they are limited by several experimental conditions, namely, the long reaction times imposed by the guest substitution step, which is in turn limited by molecular diffusion into the solid host structure. This disqualifies the use of molecular counterparts that exhibit poor chemical stability and also narrows the suitable range of size and charge of the guest entities. A workaround for these limitations may be found in the delamination/flocculation strategy. This approach consists in the exfoliation of layered inorganic solids, defined as their segregation into single entities

through soft chemistry methods.⁵ Dispersion of the appropriate layered host in a convenient liquid medium may lead to the solvation of atomically thin solid sheets and consequent formation of a stable colloidal sol.⁶ These 2D nanosheets (2DNs) can form a very interesting and versatile type of building block since they can retain the physical properties of the pristine bulk materials or even present new phenomena typical of the nanoscale realm. Subsequent flocculation of such colloids in the presence of a functional counterpart can be regarded as a promising versatile synthetic alternative for the fabrication of multifunctional hybrid materials. The exfoliation of layered hosts has hence opened the door for the construction of advanced materials that combine more sophisticated physical properties by chemical design, that is, by the appropriate choice of building blocks and the precise control of their arrangement in the solid state.⁷ This methodology has for instance permitted researchers to design hybrid superconductors in which the superconducting properties coming from the TaS₂ layers are combined with the magnetic properties coming from a magnetic component or a single-molecule magnet.^{8,9}

With the aim of extending such a methodology to other magnetic molecules, in this work we have explored the insertion of a spin crossover (SCO) complex in between superconducting TaS₂ layers.¹⁰ SCO transitions are of importance

Received: February 6, 2013

Published: July 9, 2013

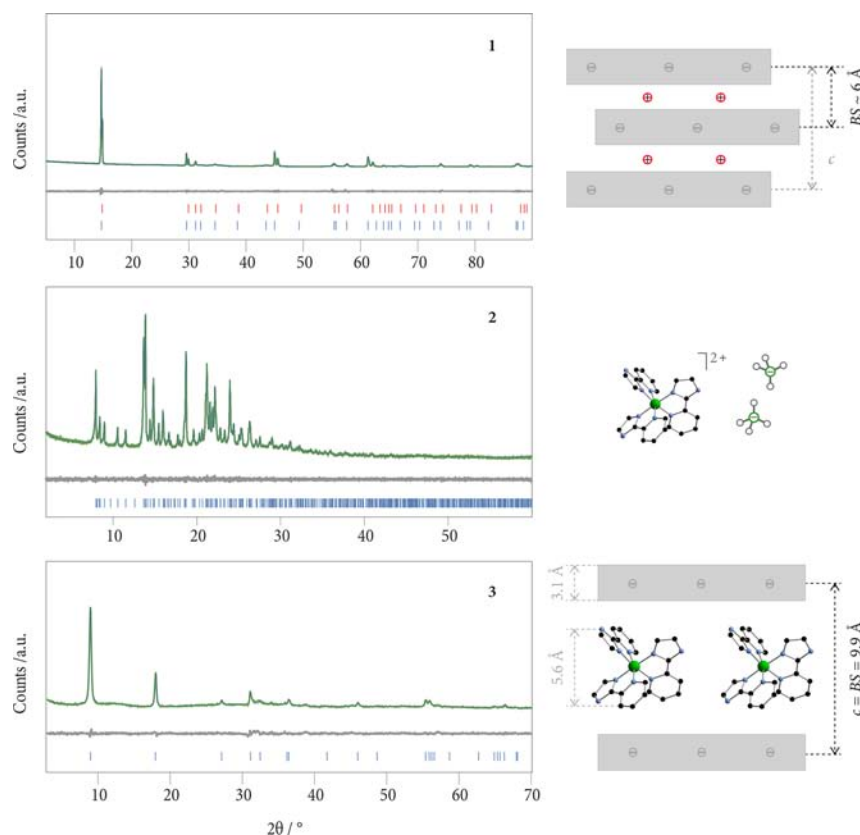


Figure 1. XRPD patterns (Cu $K\alpha_1 + K\alpha_2$) and corresponding Pawley refinements (green, observed; blue, calculated; gray, difference plot [$I_{\text{obs}} - I_{\text{calcd}}$]) of precursor Na-intercalate **1** (top), SCO complex **2** (middle), and hybrid material **3** (bottom). Cartoons of the proposed structural models of all three compounds are shown on the right.

as they may be utilized for practical switching or displaying applications. On a more fundamental note, much research has already been devoted to the understanding of spin transition processes in solid materials and also to the investigation of pathways for the control of such phenomena by either chemical design or external stimuli.¹¹

Recent activity in the field is being focused on the design of new materials in which SCO properties are blended with other chemical or physical properties.¹² For instance, the interplay between magnetism and SCO has been extensively addressed during the past few years.¹³ Electrical conductivity is another property that has also drawn much attention during the past decades in the field of molecule-based materials.¹⁴ Much effort has been dedicated to the synthesis of conducting or even superconducting organic phases composed of charge transfer complexes or radical ions.¹⁵ As a matter of fact, the combination of SCO transitions and electrical conductivity has already been explored in the past using an all-molecular approach. As conducting precursors, radical anions as well as metal complexes with redox active ligands have been used.^{16,17} Still, this approach has often afforded hybrid materials which behave as insulators or as semiconductors, at best. Thus, no real SCO metallic conductor has been so far reported, nor a SCO hybrid material exhibiting superconducting properties.

Here we show how the exfoliation/restacking approach permits combining superconductivity with SCO switching. The strategy successfully employs both solid-state and molecule-based building blocks in the assembly of a new hybrid material of general formula $[\text{Fe}(\text{L})_3]_{0.1}[\text{TaS}_2]$ (L = N-donor ligand PymH). The conducting/superconducting and SCO properties

are introduced by $[\text{TaS}_2]^{0.2-}$ 2DNs and cationic $[\text{Fe}(\text{L})_3]^{2+}$ complexes, respectively. The resulting material exhibits superconductivity below 4.5 K and gradual SCO in the 4–400 K range. Moreover, the influence of the confinement of the iron complexes on their SCO behavior is also addressed.

EXPERIMENTAL SECTION

Synthesis. All chemicals and solvents employed were of commercially available grade and were used without any previous purification. In order to ensure an inert atmosphere where required, standard Ar/vacuum line techniques were employed. The ligand 2-(1H-imidazol-2-yl)pyridine was synthesized by the general method of Radziszewskias described by Chiswell, Lions, and Morris.^{18,19} **Caution!** Perchlorate salts are potentially explosive and should be handled with care.

$\text{Na}_{0.015}\text{TaS}_2$ (1**).** This compound was prepared by the procedure described by Fang et al. with minor modifications.²⁶ Stoichiometric ratios of tantalum (2.422 g Aldrich 99.99% trace metals basis, 13.4 mmol), sulfur (0.858 g Aldrich 99.998% trace metals basis, 26.8 mmol) and sodium chloride (0.117 g Aldrich 99.999% trace metals basis, 2 mmol) were comprehensively mixed with the help of pestle and mortar and put into an Ar-purged evacuated quartz ampule (length = 25 cm; internal diameter = 15 mm; 5×10^{-5} mbar internal pressure). The system was transferred to a ceramic furnace and thermally treated as follows: 1) Heating from room temperature up to 900 °C at 5 °C.min⁻¹; 2) Constant heating at 900 °C during 48 h; 3) Cooling from 900 °C down to 700 °C at 2 °C.min⁻¹; 4) Cooling down to room temperature. The resulting black glittery solid was purified from traces of elemental sulfur by simple sublimation at 300 °C during two days. Finally, the resulting powder was thoroughly washed with distilled water to eliminate the excess nonintercalated salt crystals. The final free-flowing polycrystalline material was stored under Ar atmosphere. Phase purity was established by X-ray powder diffraction (see Figure 1). Elemental ratio estimated by XPS (calculated for $\text{Na}_{0.015}\text{TaS}_2$):

Na/Ta = 0.015 (0.015). Elemental ratios estimated by SEM-EPMA (calculated for Na_{0.015}TaS₂): Na/Ta = 0.008 (0.015); S/Ta = 1.98 (2.00).

[Fe(PyimH)₃](ClO₄)₂ (2) (PyimH = 2-(1H-imidazol-2-yl)pyridine; C₈H₇N₃). The bulk [Fe(PyimH)₃](ClO₄)₂·H₂O complex was prepared according to a procedure reported in the literature with some modifications.¹⁹ Solutions of PyimH (2.2 g) in previously degassed hot ethanol (20 mL) and Fe(ClO₄)₂·6H₂O (1.8 g) in deionized water (10 mL) were mixed and stirred at room temperature for 3 h under Ar atmosphere. The dark red solution was concentrated to half-volume on heating in an open atmosphere while bubbling Ar. After cooling down to room temperature, the complex was isolated as a polycrystalline powder induced by scratching of the inner surface of the glass. Recrystallization from a 1:1 (v/v) mixture of hot ethanol and water afforded dark red crystals. Phase purity was established by X-ray powder diffraction (see Figure 1). Anal. Calcd (%) for Fe₁C₂₄H₂₃N₉Cl₂O₉: N, 17.8; C 40.70; H, 3.27. Found (%): N, 17.80; C, 40.27; H, 3.25. ESI-MS (*F*_w = 708.25): [Fe(PyimH)₃]²⁺ and [Fe(PyimH)₃](ClO₄)⁺ at *m/z* 245.62 and 445.18, respectively. FT-IR (KBr pellet, cm⁻¹): 3417 (s), 3059 (vs), 2921 (s), 2760 (s), 1707 (m), 1615(s), 1567 (m), 1496 (s), 1470 (vs), 1450 (m), 1294 (w), 1145 (vs), 1110 (vs), 1089 (vs), 966 (w), 931 (w), 789 (s), 753 (s), 705 (s), 636 (m), 626 (s).

[Fe(PyimH)₃]_{0.1}[TaS₂] (3). The superconducting-SCO hybrid was prepared by exfoliation–flocculation such as previously reported,⁹ but this time taking special care of performing all manipulations under an inert atmosphere. Other slight modifications in the concentrations are described in the following details. Typically, 100 mg of Na_{0.015}TaS₂ black powder (0.4 mmol) was delaminated in 70 mL of a 1:1 (v/v) mixture of ultrapure Milli-Q water and *N*-methylformamide (NMF), and flocculated by dropwise addition of 2 mL of a 75 mM [Fe(PyimH)₃](ClO₄)₂ solution (0.15 mmol) in NMF. The black sediment was then washed thrice by resuspension–decantation with 20 mL of fresh ethanol and immediately dried *in vacuo*. The material was recovered as in the form of glittery light gray thin scales and was best preserved under Ar atmosphere. Phase purity was established by X-ray powder diffraction (see Figure 1). Elemental ratio estimated by EPMA (calcd for C_{2.4}H_{2.3}N_{0.9}Fe_{0.1}Ta₁S₂): Na/Ta = 0.01 (0.00), Cl/Ta = 0.00 (0.00), Fe/Ta = 0.10 (0.10), Ta/S = 0.78 (0.5).

Physical Characterization. Metallic composition of bulk samples was estimated by electron probe microanalysis (EPMA) performed in a Philips SEM XL30 equipped with an EDAX microprobe. Carbon, nitrogen, and hydrogen contents were determined by microanalytical procedures using an EA 1110 CHNS-O elemental analyzer from CE Instruments. Infrared spectra were recorded in a FT-IR Nicolet 5700 spectrometer in the 4000–400 cm⁻¹ range using powdered samples diluted in KBr pellets. Particle morphologies and dimensions were studied with Hitachi S-4800 FE-SEM operated at 20 kV, over metalized samples with a mixture of gold and palladium during 30 s. Thermogravimetric analysis of all compounds were carried out with a Mettler Toledo TGA/SDTA 851 apparatus in the 25–800 °C temperature range under a 10 °C min⁻¹ scan rate and an air flow of 30 mL min⁻¹.

X-ray powder diffraction (XRPD) patterns were collected with a Bruker D8 Advance X-ray diffractometer (Cu Kα1/Kα2 radiation; λ_{α1} = 1.540 60 Å, λ_{α2} = 1.544 34 Å) operating at 80 mA and 45 kV equipped with a LYNXEYE XE 1-D detector. Samples were mounted on a corrugated PMMA specimen holder ring in a θ–θ reflection geometry. Profiles were generally collected in the 5° < 2θ < 90° range with a typical step size of 0.02°. Transmission measurements were performed on a Empyrean PANalytical powder diffractometer, using Cu Kα radiation (λ = 1.541 77 Å). Polycrystalline samples of 1–3 were lightly ground in an agate mortar and pestle and filled into 0.5 mm borosilicate capillaries. Data were collected at room temperature in the 2θ ranges 5–90° (1), 2–60° (2), and 3–70° (3). Pawley refinements were performed using the TOPAS computer program.^{20,21}

Conventional magnetic characterization was carried out with a commercial MPMS-XL SQUID magnetometer, operating between 300 and 1.8 K.

X-ray photoelectron spectroscopy (XPS, K-ALPHA, Thermo Scientific) was used to analyze the filter surface. All spectra were collected using Al Kα radiation (1486.6 eV), monochromatized by a twin crystal monochromator, yielding a focused X-ray spot with a diameter of 400 μm, at 3 mA × 12 kV. The alpha hemispherical analyzer was operated in the constant energy mode with survey scan pass energies of 200 eV to measure the whole energy band and 50 eV in a narrow scan to selectively measure the particular elements. Charge compensation was achieved with the system flood gun that provides low energy electrons and low energy argon ions from a single source. XPS depth profiles were obtained by sputtering the specimen with a 3 keV Ar⁺ ion beam during periods of 30 s. The analysis spot was elliptical in shape with a major axis length of 400 μm. XPS data was analyzed with Avantage software; a Shirley background function was used to approximate the experimental backgrounds, and surface elemental compositions were calculated from background-subtracted peak areas.

Mössbauer spectra were collected in transmission mode using a conventional constant-acceleration spectrometer and a 25 mCi ⁵⁷Co source in a Rh matrix. The velocity scale was calibrated using α-Fe foil. The absorbers were obtained by packing the powdered samples into perspex holders. Isomer shifts are given relative to metallic α-Fe at room temperature. The spectra at 4 and 2 K were collected using a bath cryostat with the sample immersed in liquid He. The spectra were fitted to Lorentzian lines using a nonlinear least-squares method.²²

The electrical conductivity (σ) measurements of 3 have been performed using a standard four-probe method with Pt wire in a physical properties measurement system (PPMS-9) by Quantum Design. Electrical contacts were made with highly conducting silver and on sample sizes of approximately 9.37 × 10⁻³ cm².

RESULTS AND DISCUSSION

Chemical Design. As layered solid-state host, we have focused on the classical transition metal dichalcogenide (TMDC) family.²³ Among them, TaS₂ suited particularly well our purposes in being a stable and robust member of the TMDC family, which presents metallic conductivity down to a critical temperature (*T*_{SC}) of 0.6 K when a transition to the Meissner superconducting state occurs. From a structural point of view, TaS₂ is as a layered material made out of stacks of neutral weakly interacting single layers much in the fashion of graphite. Interestingly, the synthesis of nonstoichiometric Na_xTaS₂ phases from its elemental components in the solid state has been previously reported.²⁴ These “intercalation”²⁵ materials present interesting properties different from the neutral TaS₂ parent material. Indeed, the temperature for which superconductivity is observed increases from around 0.6 K, for the neutral pristine 2H tantalum disulfide phase, up to around 4 K depending on the degree of doping.²⁴ Additionally, the chemically injected charge that is confined within the TaS₂^{x-} planes enhances the interlayer electrostatic repulsion and favors solvation processes. This may be utilized to try and isolate individual layers,²⁶ making the material an ideal candidate for undertaking delamination/flocculation. In this way, a stable sol of anionic superconducting highly anisotropic solvated nano-sheets may be restacked by the addition of a functional cationic complex. This opens the door for the combination of the inherent superconductivity provided by the [TaS₂]^{x-} anionic layers with the SCO features introduced by a cationic metal complex.

As SCO cationic species we focused on classical Fe²⁺ octahedral complexes of N-donor ligands. A big number of these compounds present clean SCO transitions with large bistability regions.²⁷ In particular, Fe(PyimH)₃](ClO₄)₂ (PyimH = 2-(1H-imidazol-2-yl)pyridine; C₈H₇N₃) not only presents a relatively abrupt spin transition above room

temperature but also may be switched by light radiation stimuli.²⁸ The SCO precursor is a simple single-ion complex that lives up to the few requisites imposed by the delamination/flocculation approach: it is a stable cation, which is soluble in the polar protic solvents that will be used for the wet exfoliation of the host material.

Synthesis and Structure. Na_xTaS₂ (**1**) was prepared from the ceramic reaction of a stoichiometric mixture of elemental Ta and S and ultrapure NaCl according to the methodology previously reported by Fang et al.²⁴ Formerly, Na-intercalated phases for the synthesis of hybrid materials were accessed via a two-step process that began with the synthesis of pure 2H-TaS₂ and ended with the wet topotactic reduction of the pristine neutral material.^{7,8} In contrast, the approach used here permits saving both time and resources, and most importantly, it greatly improves the integrity of the precursor Na-intercalated material. As a matter of fact, Na_{0.33}TaS₂ crystallites synthesized via basic reduction exhibited rounded crystallite vertex and more irregular facets as seen by SEM (see Supporting Information, S11). These features result from mechanical and chemical erosion associated to the wet intercalation reaction. Additionally, Na_{0.33}TaS₂ synthesized via topotactic reduction also showed a decrease in the overall crystallinity of the sample if compared with TaS₂ pristine samples. This is attributed to the larger turbostratic disorder in the *ab*-plane that results from the intercalation reaction and gallery height enlargement.²⁹ On the contrary X-ray powder diffraction (XRPD) pattern of bulk samples of **1** showed extremely intense and sharp diffraction peaks (Figure 1). The large aspect ratio of the sample crystallites resulted in preferred orientation of powder specimens, making it difficult to observe diffraction peaks other than the (00*l*) family in a θ - θ reflection geometry experiment (see Supporting Information, S12). Nevertheless, indexation of the mentioned reflections by assuming a hexagonal symmetry allowed for the identification of two very similar phases with the following *c*-axis unit cell parameters: $c^A = 12.089\ 80(19)$ Å and $c^B = 11.9497(2)$ Å (see Table 1). Phase A coincides with

Table 1. Unit Cell Parameters from Pawley Refinements for Compounds 1, 2, and 3 and Those of Analogous Compounds from Single Crystal Diffraction Data

| | <i>a, b</i> /Å | <i>c</i> /Å | α, β /deg | γ /deg | BS/Å |
|--|----------------|--------------|----------------------|---------------|------|
| 1 ^A | 3.31708(14) | 12.08980(19) | 90 | 120 | 6.04 |
| 1 ^B | 3.313(2) | 11.9497(2) | 90 | 120 | 5.97 |
| 2H-TaS ₂ ^a | 3.315 | 12.10 | 90 | 120 | 6.50 |
| 2 | 12.8058(11) | 63.702(7) | 90 | 120 | |
| [Fe(PyimH) ₃] (ClO ₄) ₂ ·H ₂ O ^b | 12.7633(5) | 63.459(5) | 90 | 120 | |
| 3 | 3.3150(6) | 9.863(19) | 90 | 120 | 9.86 |

^aJellinek, F. J. *Less-Common Met.* **1962**, *4*, 9–15. ^bCoronado, E.; Giménez-Marqués, M.; Mínguez Espallargas, G. Unpublished work.

that described in the literature for single crystals of Na_xTaS₂.²⁶ On the other hand, phase B shows a basal spacing that is very similar to that reported for 2H-TaS₂. This provides evidence for the fact that most Na⁺ ions remain away from the bidimensional galleries. In order to diminish the effect of preferred orientation and to try to enhance the in-plane family of reflections, the sample was loaded into a glass capillary, and a transmission XRPD pattern was collected (top panel of Figure 1). Though still faint, transmission data permitted identifying

the (100) and (010) reflections. The Pawley refinement of this powder pattern revealed an excellent fit to a two-phase model ($R_{wp} = 0.0697$; $R_{wp}' = 0.1469$ and $GOF = 1.815$; R_{wp}' is the background subtracted R_{wp}) with a hexagonal cell with $a = 3.31$ Å in agreement with that described for TaS₂ layers with trigonal prismatic Ta coordination such as 2H-TaS₂. Homogeneous morphology of the isolated Na_xTaS₂ microcrystals was confirmed with SEM (Supporting Information, S11). Hexagonal-shaped crystals were approximately 100 μm in length and 20 μm in thickness. Given the small ratio of Na in the isolated sample, EPMA lacked sensitivity and was not a suitable probe for stoichiometry determination. Thus, the chemical composition of the bulk samples of **1** was determined via XPS. An overall Na/Ta ratio of 0.015 ± 0.005 could be inferred (see Supporting Information, S13).

To our knowledge, no previous works on the solvent-based exfoliation of such small-gallery-height Na-intercalates have been reported. In order to investigate the wet exfoliation of **1**, delamination tests were carried out on bulk samples. For that purpose, pristine polycrystalline samples of Na_{0.015}TaS₂ were immersed in degassed water/*N*-methylformamide 50% (v/v) mixtures under an argon inert atmosphere and were treated with recurrent cycles of mechanical stirring and sonication. Indeed, it was found out that the behavior of **1** was comparable to that of other Na-intercalated phases synthesized by wet techniques. In this line, after a long ultrasound cycle, the anionic [TaS₂]^{0.015-} nanoflake sol had attained remarkable stability and did not sediment readily (see Supporting Information, S14), and stable sols with maximum effective colloidal concentration of 0.35 g/L could be achieved. The exfoliated nanosheets appear as high aspect ratio flakes as seen by HR-TEM (see Supporting Information, S14). The weak homogeneous contrast exhibited by TEM images suggests uniform nanometric thickness. The technique permitted us to verify the structural integrity of the isolated flakes. At this stage, the [TaS₂]^{0.015-} is ready for flocculation with the cationic counterpart. It is also important to underline how crucial it is to carry out the exfoliation process under inert conditions. The argon atmosphere not only favored a clean delamination process but also prevented oxidation processes in the subsequent flocculation step.

The Fe²⁺ complex [Fe(PyimH)₃](ClO₄)₂ was obtained as a burgundy crystalline powder in excellent yields, and chemical composition was confirmed through elemental, XRPD, and FT-IR studies (view Figure 1 and Supporting Information, S15).

The flocculation of [Fe(PyimH)₃]-TaS₂ hybrid **3** was performed under an argon inert atmosphere to prevent the oxidation of the redox-active counterparts involved in the reaction. In this way, solvents were thoroughly degassed, and reaction vessels were conveniently flushed with Ar. Other than that precaution, the rest of the flocculation was carried out as reported by us in previous works. The flocculation of **3** always occurred under an excess of [Fe(PyimH)₃]²⁺. It is important to realize that the process is driven by attractive electrostatic interactions between the oppositely charged species that coexist in solution until electroneutrality is achieved. Thus, the excess [Fe(PyimH)₃]²⁺ always remained soluble in the supernatant and needed to be discarded by decantation. The isolation of a pure crystalline phase of general formula [Fe(PyimH)₃]_y[TaS₂] was achieved by this procedure. The theoretical stoichiometry expected from electroneutrality calculations suggests an approximate value of $y = 0.007$. Yet, the empirical formula estimated on the basis of SEM EPMA metal analysis (see

Supporting Information, SI3) reflected a larger proportion of Fe with respect to the proposed one. Thus, a value of $y = 0.1$ could be inferred from metallic ratio data extracted from SEM spectra. This metallic ratio was found to be constant despite the flocculated slurry being always thoroughly rinsed with fresh solvent in order to wash away remaining precursor coprecipitated impurities. In addition, no Na or Cl could be detected by EPMA, thus ruling out the presence of Na-intercalated **1** or perchlorate salt **2** precursor leftovers. The mismatch between the theoretical and the experimentally calculated metallic ratios may be explained by a redox process that involves the partial reduction of the $[\text{TaS}_2]^{0.015-}$ nanoflakes. As a result, the nanolayers acquire a higher charge, namely -0.2 , and require a larger number of counteranions for electrostatically restacking. Due to the fact that the whole process was carried out under an inert atmosphere, it is proposed that the reducing agent came from the reaction medium itself. This hypothesis is consistent with Mössbauer and XPS studies, which clearly revealed the presence of oxidized Fe^{III} species in the final hybrid (*vide infra*). This means that a certain proportion of these Fe species are trapped inside the layered structure of the final hybrid along with other pristine Fe^{II} complexes. The remaining excess Fe complex molecules are discarded in the supernatant solution.

If no extra care was taken during filtration and isolation steps, hybrid compound **3** could be obtained as a powder sample. Alternatively, the isolation of the final hybrid material could also be achieved in the form of free-standing highly oriented macroscopic flakes. The slow controlled sedimentation of the flocculated material followed by vacuum filtration on $0.2 \mu\text{m}$ pore size Teflon (polytetrafluoroethylene, PTFE) membranes yielded large surface area thin scales (typically several $\text{mm}^2 \times 5 \mu\text{m}$ thick) that could be easily removed from the filter surface. Closer examination under SEM reveals that the flocculated high aspect ratio layers appear to have the same orientation, with the crystallographic c axis normal to the flake plane as opposed to powder samples where crystallite orientation was random (see Supporting Information, SI6). These samples were most convenient for conducting transport measurements since the preparation of pressed pellets that has been reported to destroy superconductivity in TMDCs was not required.^{8,9,30} They are also ideal candidates for the characterization of anisotropic physical properties such as two-dimensional superconductivity.

Evaluation of the XRPD profiles collected from ground samples of **3** together with those of the starting materials (**1** and **2**) agrees with the creation of a different and pure layered crystalline phase from the combination of the ionic 2DNs and the Fe^{2+} complexes in solution (see Figure 1). Furthermore, the Pawley refinement of the X-ray diffraction data indicates that there is a unique layered-dichalcogenide-type crystalline phase present in **3** in contrast to starting material **1** where two different phases are found (see Table 1). This reinforces the idea of a successful restacking process to produce a totally different layered material. Inherent to the rapid flocculation methodologies employed for the nanolayer restacking, **3** presents a bigger number of stacking defects and overall disorder than the starting components. This is suggested by the weaker intensity and broader full widths at half-maximum (fwhm) of its diffraction peaks in comparison to the precursor materials'. In the past these complications have impeded the postulation of consistent structural models for the intercalation compounds of layered dichalcogenides.³¹ However, in our case the Pawley refinement of the diffractogram of **3** permitted

estimating the following hexagonal ($\alpha = \beta = 90^\circ$, $\gamma = 120^\circ$) unit cell: $a = 3.3150(6) \text{ \AA}$, $c = 9.863(19) \text{ \AA}$. It is presumed that the 2H stacking conformation of the layers with an alternating packing of two crystallographically distinct TaS_2 slabs turns into a phase with a single TaS_2 layer in the unit cell as has already been reported for similar delamination/flocculation processes.⁸ Such a single-layer stacking periodicity provides a $BS = c$ of ca. 9.9 \AA for **3**. This is in good accordance with the addition of the thicknesses of one layer of TaS_2 , 3.1 \AA ,³² and the size of the Fe^{2+} complex inserted with its C_3 axis perpendicular to the TaS_2 planes (Figure 1). In addition, the hexagonal a -axis of $3.3150(6) \text{ \AA}$ supports that the hybrid layered structure is sustained by unaltered TaS_2 individual planes.³³ Unfortunately, the structural data does not permit giving any further information regarding the distribution of the SCO cations within the bidimensional space afforded by the TaS_2 planes. Nevertheless, in view of the stoichiometry of the hybrid material together with the surface charge density of the $[\text{TaS}_2]^{0.2-}$ planes, it is evident that Fe^{2+} centers are further apart from each other than in the precursor perchlorate salt. Simple surface charge calculations (see Supporting Information, SI7), taking into account the 2H- TaS_2 in-plane structure, permit establishing that each SCO molecule bearing two positive charges occupies an average area of 200 \AA^2 within the interlayer gallery. This suggests an efficient segregation of the Fe^{2+} complexes, which should have a direct effect over the cooperativity of the SCO phenomenon.

Mössbauer. Mössbauer experiments were carried out for 100% ^{57}Fe enriched samples of **2** and **3** in order to study the SCO transitions (Figure 2). The 295 K spectrum of **2** consists of three absorption peaks which may be fitted with two quadrupole doublets while at 4 K only one doublet is observed. The estimated isomer shifts relative to αFe at 295 K (IS) and quadrupole splittings (QS) are shown in Table 2. The doublet with lower IS and QS corresponds to low spin (LS) Fe^{II} ($S = 0$), and the doublet with higher IS and QS detected at 295 K, to high spin (HS) Fe^{II} ($S = 2$) in agreement with reported results for similar Fe^{II} SCO complexes such as $[\text{Fe}(\text{bpp})_2]^+$: $[\text{Fe}(\text{bpp})_2](\text{BF}_4)$,³⁴ $[\text{Fe}(\text{bpp})_2](\text{CF}_3\text{SO}_3)_2 \cdot \text{H}_2\text{O}$,³⁵ $[\text{Fe}(\text{bpp})_2][\text{MnCr}(\text{ox})_3]_2$.³⁶ The spectra of **2** evidence a spin crossover transition showing that all the Fe^{II} is LS at 4 K and only approximately 15% is HS at 295 K. As reported by Vijayalakshmi et al., this compound was also found to mainly exhibit LS state at room temperature.³⁷ Since our sample was 100% enriched in ^{57}Fe , a spectrum with better statistics could be obtained, which allowed the detection of the HS state at 295 K.

The 4 K spectrum of **3** reveals, in addition to both doublets assigned to LS and HS Fe^{II} , the presence of a sextet with broad peaks. This sextet becomes more evident at 2 K. The IS ($\sim 0.48 \text{ mm/s}$) and magnetic hyperfine field B_{hf} ($50.1\text{--}51.6 \text{ T}$) estimated for this sextet (Table 2) are typical of HS Fe^{III} . Mössbauer spectra therefore confirm that Fe^{2+} is partially oxidized even when the synthesis was performed under an inert atmosphere. This further supports the hypothesis of an internal redox event between the host layers and the guest Fe complexes. The fact that the broad peaks of this sextet are only observed at 4 K and below suggests that the sextet results from a slowing down of the relaxation frequency of the Fe^{III} magnetic moments directions below the Larmor precession frequency ($f_L \sim 4 \times 10^7 \text{ Hz}$) of the ^{57}Fe nuclei.³⁸ At temperatures higher than 4 K the relaxation is faster than f_L and a doublet is observed instead. This slow relaxation is not caused

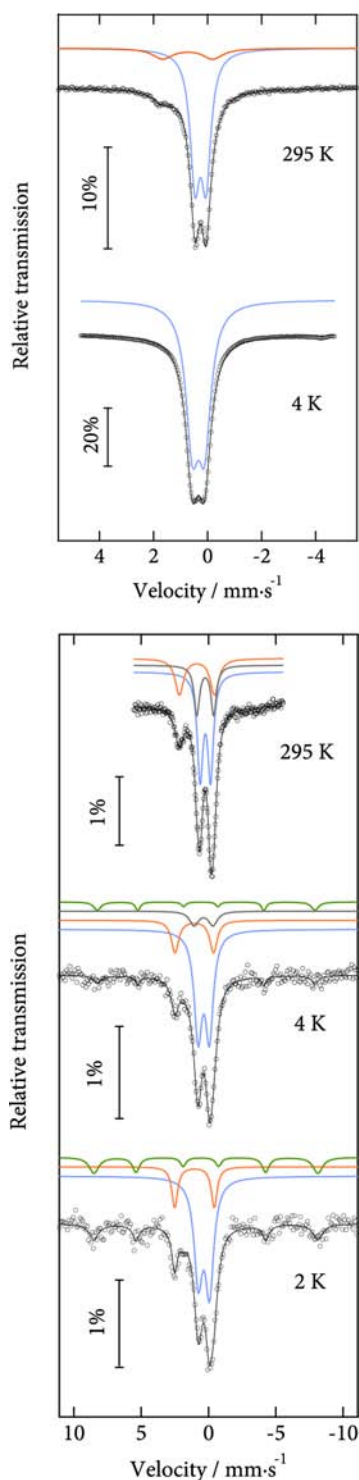


Figure 2. Mössbauer spectra of 2 (top) and 3 (bottom) recorded at different temperatures.

by magnetic ordering but results from a slow spin–spin relaxation of the HS Fe^{III} cations caused by the large Fe^{III}–Fe^{III} distances in 3. The absence of a magnetic moment for LS Fe^{II} and the spin–lattice relaxation mechanism available to HS Fe^{II} due to spin–orbit coupling may explain why no slow relaxation is observed for Fe^{II}.³⁸

The Fe^{III} doublet that is expected at room temperature is not resolved from the LS Fe^{II} doublet due to similar IS and QS values. In order to estimate the fractions of Fe^{II} HS and LS at

Table 2. Estimated Parameters of 2 and 3 Extracted from the Mössbauer Spectra Taken at Different Temperatures^a

| T/K | IS/mm s ⁻¹ | QS/mm s ⁻¹ | B _{hf} /T | Γ/mm s ⁻¹ | I% | Fe state |
|----------|-----------------------|-----------------------|--------------------|----------------------|-----|---------------------|
| 2 | | | | | | |
| 295 | 0.37 | 0.41 | | 0.41 | 85 | Fe ^{II} LS |
| 295 | 0.87 | 1.87 | | 0.91 | 15 | Fe ^{II} HS |
| 4 | 0.46 | 0.45 | | 0.58 | 100 | Fe ^{II} LS |
| 3 | | | | | | |
| 295 | 0.35 | 0.78 | | 0.51 | 49 | Fe ^{II} LS |
| 295 | 0.97 | 2.60 | | 0.75 | 25 | Fe ^{II} HS |
| 295 | 0.35 | 1.25 | | 0.48 | 26 | Fe ^{III} |
| 4 | 0.46 | 0.84 | | 0.70 | 63 | Fe ^{II} LS |
| 4 | 1.16 | 2.86 | | 0.66 | 17 | Fe ^{II} HS |
| 4 | 0.48 | 1.40 | | 0.78 | 11 | Fe ^{III} |
| 4 | 0.48 | -0.40 | 50.1 | 0.38 | 9 | Fe ^{III} |
| 2 | 0.45 | 0.83 | | 0.75 | 62 | Fe ^{II} LS |
| 2 | 1.15 | 2.94 | | 0.51 | 17 | Fe ^{II} HS |
| 2 | 0.49 | -0.38 | 51.6 | 0.50 | 21 | Fe ^{III} |

^aIS isomer shift relative to metallic α -Fe at 295 K; QS quadrupole splitting; B_{hf} magnetic hyperfine field; Γ width; I relative areas. Estimated errors are ≤ 0.02 mm/s for IS, QS, Γ ; ≤ 0.5 T for B_{hf}; and $\leq 2\%$ for I.

295 K the data analysis was performed assuming the presence of three doublets at this temperature. Such a fitting leads to parameters consistent with those observed at 2 K. The IS for each Fe species is lower according to the second-order Doppler shift. The relative area of the Fe^{III} doublet is slightly higher than the relative area of the Fe^{III} sextet at 4 K, which may be explained by a higher recoil-free fraction of Fe^{III} relative to Fe^{II}.

The lower area of the Fe^{III} sextet at 4 K when compared to 2 K suggests that at 4 K a fraction of the Fe^{III} still has a relaxation faster than f_L and is giving rise to a doublet. The analysis of the spectra indicates that this fraction corresponds to approximately half of the Fe^{III} (Table 2). The estimated fraction of Fe^{II} in HS state is approximately 22–23% at 4 and 2 K and approximately 34% at room temperature evidencing SCO in the 4–295 K temperature range.

Mössbauer spectra show that the IS value of LS Fe^{II} in the [Fe^{II}(PyimH)₃]²⁺ complex does not change within experimental error when this complex is inserted between TaS₂ layers. IS of HS Fe^{II} however increases. Such increase normally indicates an increase in the ionic character of the chemical bond (decrease in the 4s electron density of the formal Fe²⁺ or alternatively increase in 3d electron density that results in a higher shielding of the s electrons relative to the Fe nuclei). Furthermore the QS of both LS and HS Fe^{II} are higher in compound 3 than in 2 which means that insertion of the [Fe^{II}(PyimH)₃]²⁺ complex between the TaS₂ layers increase the distortion of the charge distribution around the Fe^{II}. This may explain the different SCO behavior of [Fe^{II}(PyimH)₃]²⁺ in 3 and in 2, particularly the fact that HS Fe^{II} is still observed at 2 K in 3 while in 2 all the Fe^{II} is LS. It is suggested that this observation may be a direct consequence of the confinement of the metal complexes within the TaS₂ layered architecture.

Magnetic Properties. The variation of ac susceptibility with temperature of precursor material 1 was surveyed to serve as a reference for comparison with the synthesized hybrid material and also for further confirmation of the quality of the starting material (see Supporting Information, SI8). Powder samples of 1 showed a sharp transition to the superconducting state below $T_{SC} = 3.2$ K indicative of a pure and crystalline

Na_xTaS_2 2H phase with $0 < x < 0.05$.²⁶ This ties in correctly with the value of $x = 0.015$ determined by XPS data (*vide supra*). Magnetization curves were recorded under increasing ac external fields. The data allowed for the rough estimation of the type II superconductor upper critical field (H_{c2}) at which 100% volume of the material has switched to the normal state. A value of 1400 Oe could be extracted from the onset point of both the asymptotically decreasing out-of-phase curve and the increasing in-phase component.

Next, the thermal variation of ac susceptibility of hybrid material **3** was recorded in the 300–2 K temperature range (Figure 3). The ac behavior is characterized by a drop of the in-phase ac susceptibility, χ' , and a maximum in the out-of-phase component, χ'' , both being long-range frequency independent features. In this case, the sharp fall of the ac susceptibility at T_{SC}

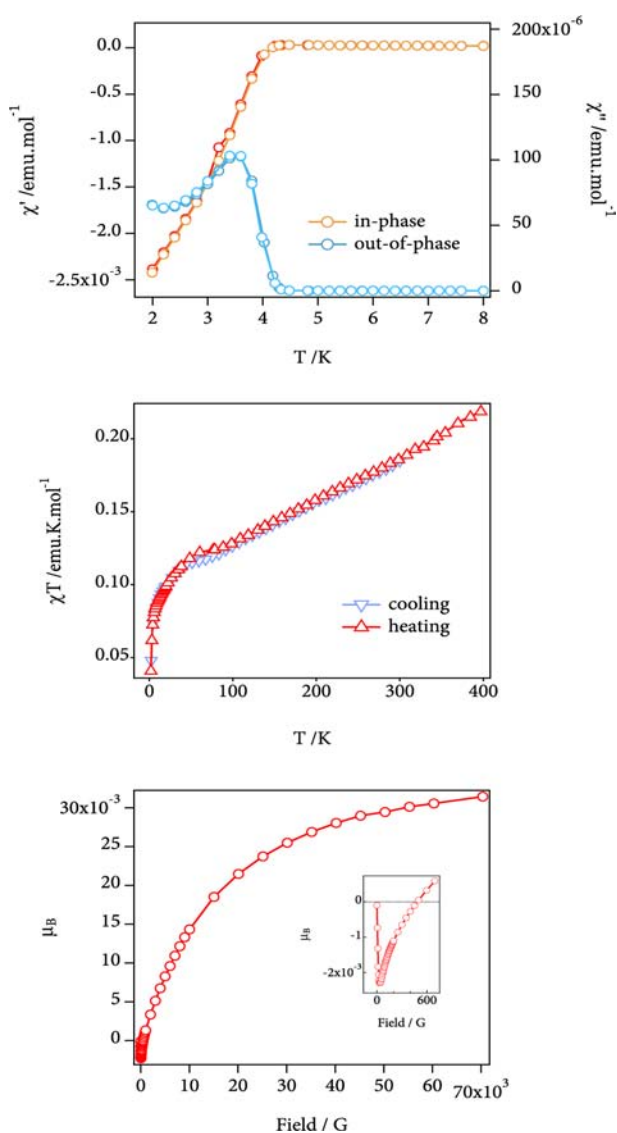


Figure 3. Magnetic characterization of hybrid sample **3**. Top: ac magnetic susceptibility thermal variation from 8 to 2 K measured at two different frequencies (110 and 1 Hz) at zero external applied field. Middle: χT product versus T heating/cooling cycles measured under 1000 G of external applied field in the 300–2 K temperature range. Bottom: Magnetization curve measured at 2 K. The inset presents a close up of the low-field region to show the typical features of a type II superconductor.

is representative of unaltered nanolayers that persist in the restacked material. This is demonstrative of how the superconducting properties have been successfully brought into the final material. However, although the in-phase and out-of-phase profiles of compounds **1** and **3** are comparable, they are not identical. Indeed, **3** presents a Meissner superconducting response below 4.5 K, which defines an increase in the T_{SC} of $\Delta T_{SC} = 1.3$ K with respect to the Na-intercalated precursor **1**. The explanation to this increase in T_{SC} may be found in the mentioned partial reduction of the $[\text{TaS}_2]^{-0.015}$ to a higher charged state $n = -0.2$. This is once again consistent with both a partial oxidation of the Fe^{2+} centers illustrated by Mössbauer spectroscopy and with the nonideal stoichiometry found in the chemical analysis and XPS results. It is also in perfect agreement with the superconducting critical temperature expected for $[\text{TaS}_2]^{-0.2}$ ($T_{SC} = 4.3$ K) reported in the literature.²⁶ Field expulsion experiments were conducted in the presence of increasing dc external applied fields in the 6–2 K range (Supporting Information, SI9). In this way, ac susceptibility thermal variations were collected under the effect of varying dc external applied fields. In-phase profiles show how the Meissner effect is gradually annihilated as the external applied field approaches the critical field H_{c2} . At the same time, the peak exhibited by χ'' , at zero applied field, is gradually smeared out upon increasing the external dc value. The results also allowed for the estimation of the critical field inherent to the superconducting component of the hybrid material. Conventionally, this can be extracted from magnetization studies. However, in our hybrid, the paramagnetic component coming from the paramagnetic Fe centers handicapped such determination. In this case, it is interesting to note how upper critical fields for hybrid sample **3** are subtly higher than for precursor material **1**. Indeed, applied fields of around 3000 G are needed to eliminate the χ'' component of the ac susceptibility. Therefore, H_{c2} lies between 2000 and 3000 Oe. This is consistent with the increase in T_{SC} suggested by the premature onset of the ac response in zero applied field in comparison to the precursor material. Furthermore, the isolation of highly oriented flakes of material **3** allowed for the angle-dependent probing of the material's ac response. Alternating current thermal variations were recorded as a function of the angle between the flake normal and the external uniaxial field. In this way, it is easy to observe that the strong bidimensional anisotropy of the starting material is preserved in the hybrid structure. As a single flat flake of compound **3** was rotated within the dc field, ac response was maximum upon reaching an orthogonal orientation (90°) of the crystallographic c -axis with respect to the external field axis (Figure 4). At this orientation, the low-temperature susceptibility is close to the limit ($-1/(4\pi)$ emu cm^{-3}) expected for perfect diamagnetism. These results neatly show that the superconductivity observed in this material is a bulk effect, which involves nearly 100% of the sample.

Following, the SCO transition was addressed by recording the thermal variation of χT for sample **3** under 1000 G of applied external field (Figure 3). The dc profile exhibits two distinct temperature sections that must be discussed separately: the 400–4.5 K region and the 4.5–2 K one. On one hand, the higher temperature range (400–4.5 K) shows a gradual decrease in χT as the temperature falls. The χT value at 400 K of approximately 0.23 emu K mol^{-1} suggests that a complete spin transition to high-spin state has not yet been achieved at that temperature. Taking the 295 K Mössbauer spectra (Fe^{II} HS

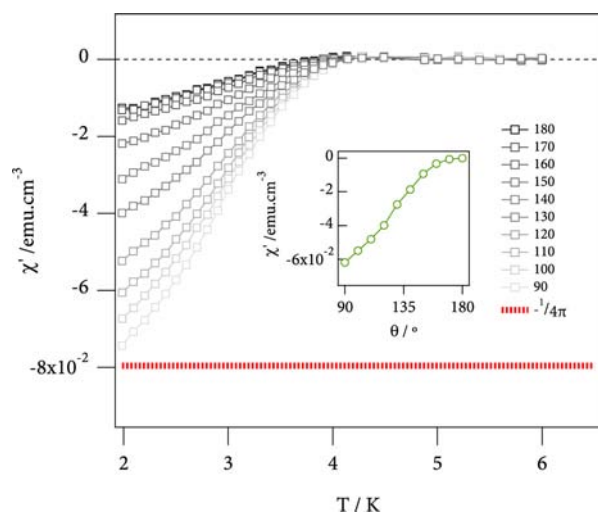


Figure 4. Alternating current in-phase magnetic susceptibility thermal variation measured at different relative orientations [specific angles (θ in deg) are listed in the legend] of a highly oriented flake of **3** with respect to the external applied field. The ideal Meissner response [horizontal red dashed line at $-1/(4\pi)$ emu cm^{-3}] is included as a reference. The inset shows the variation of the χ' value at 2 K. The sample density was calculated from the crystal structure inferred from XRPD data ($4248.28 \text{ kg m}^{-3}$).

mol/ Fe^{III} mol = 0.96) and the relative spin-only values for Fe^{II} and Fe^{III} into account, a ratio of $\chi T[\text{Fe}^{\text{II}} \text{ HS}]_{295\text{K}}/\chi T[\text{Fe}^{\text{III}}]_{295\text{K}} = 0.66$ may be deduced. The 295 K χT value of 0.20 emu K mol^{-1} may therefore be split into the paramagnetic components coming from the HS Fe^{II} (0.08 emu K mol^{-1}) and Fe^{III} (0.12 emu K mol^{-1}) species present in the hybrid material. As a matter of fact, this reveals that, at 295 K, around 20% of the Fe^{2+} centers are in their high-spin state according to the spin-only calculation for 0.1 mol high-spin Fe^{2+} per compound formula. This is consistent with Mössbauer data within experimental error. Upon decreasing the temperature, a quasilinear χT decrease follows. This progressive drop may be attributed to a gradual SCO transition down to 4.5 K. At this point, a χT value of 0.12 emu K mol^{-1} is reached. Down the lower temperature range (5–2 K), the Meissner effect starts to operate and dominate that part of the profile. The sample diamagnetism starts to build up and describes an abrupt drop of the χT product. Finally, two cooling–heating dc susceptibility cycles were performed and the corresponding susceptibility thermal variations recorded in order to explore potential spin bistability regions. The results showed no significant hysteresis in the whole temperature range, which indicates the lack of cooperative effects. This is consistent with the structural model proposed of a loose-packed organization of isolated SCO complexes within the bidimensional galleries provided by the layered host. Lastly, it is important to mention that the effect that the host Meissner state may exert over the SCO centers is difficult to evaluate via magnetic characterization given the small temperature range in which the superconductivity operates together with the SCO transition and also due to the strong diamagnetic fall at low temperatures.

The magnetization curve of sample **3** was measured at 2 K (see Figure 3). It shows a low-field minimum that originates from the diamagnetism coming from the superconducting TaS_2 layers. Upper and lower critical fields characteristic of type II superconductivity could be estimated from such feature and depicted only a subtle variation with respect to the precursor

sample **1** (see Supporting Information, SI8). As the applied field is increased above 50 G, superconductivity is gradually annihilated and finally completely suppressed at $H_{c2} \approx 220$ Oe. Superconductivity suppression gives way to the observation of a paramagnetic component, which defines a typical Brillouin function attributed to the Fe^{2+} centers that still remain in their high-spin configuration at 2 K. However, the saturation of the magnetic moment is not achieved even at 5 T so no clear conclusions regarding the remnant HS fraction of the Fe^{II} species could be drawn from these data.

XPS. XPS surface measurements performed on single crystallites of sample **1** and on hybrid **3** in the form of free-standing scales permitted analyzing the chemical states of the metallic components of the hybrid (see Figure 5). The survey of the Ta binding energy region allowed for the observation of three $4f_{7/2}$ – $4f_{5/2}$ doublets (components a–c) that could be assigned to an equal number of chemical states. Both compounds **1** and **3** exhibited an intense doublet with the $4f_{7/2}$ peak centered at around 23 eV and another less intense one positioned at approximately 24 eV. While the latter doublet

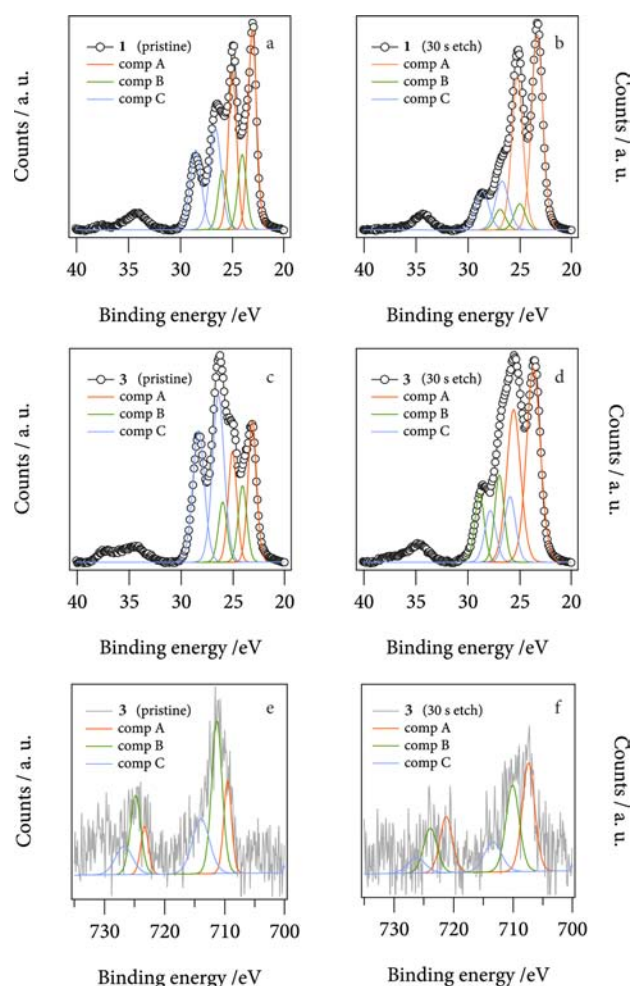


Figure 5. XPS spectra and oxidation state analysis. Ta binding energy region for **1** (a and b) and **3** (c and d). The figures on the left-hand side (a and c) were collected from the surface of as-synthesized material, whereas the graphs on the right (b and d) correspond to samples whose surfaces had been etched off with 30 s Ar^+ ion bombardment. The Fe binding energy region collected from an oriented flake of hybrid sample **3** is shown in graphs e (pristine sample) and f (etched).

exactly matches that expected for Ta⁴⁺ in neutral TaS₂ (23.9 eV), the former is shifted toward lower binding energies, indicating Ta³⁺. This reflects the n-doped state of the dichalcogenide layers with a Ta⁴⁺/Ta³⁺ mixed valence situation.³⁹ Still, no further distinctions with respect to the different degree of doping between compounds **1** and **3** could be established. On the other hand, a very intense doublet at around 26 eV depicted the presence of a much more oxidized Ta species. According to that reported in the databases, a binding energy of 26 eV coming from the 4f_{7/2} transition may be assigned to tantalum pentoxide (Ta⁵⁺).⁴⁰ This clearly demonstrates the ready superficial oxidation of the TaS₂ host that may be observed even in freshly prepared samples. In order to discard bulk oxidation of the samples, high aspect ratio samples of **1** (crystals) and **3** (oriented flakes) were etched by Ar⁺ bombarding. Indeed, spectra collected after the ion etching exhibited a much weaker Ta⁵⁺ signal and a dominating 23 eV 4f_{7/2} peak.

The Fe XPS footprint of **3** was also addressed. Despite the 2p signal being weak, the experimental profile allowed for its deconvolution in three different components. Two lower binding energy 2p_{1/2}–2p_{3/2} doublets appeared to be especially intense. These could be ascribed to the HS (2p_{3/2} = 711 eV; 2p_{1/2} = 725 eV) and LS (2p_{3/2} = 709 eV; 2p_{1/2} = 723 eV) components of the Fe²⁺ species present in the sample. A particularly high separation between both components (ca. 2 eV) is evidenced in accordance to previous studies on spin crossover Fe²⁺ compounds.⁴¹ The third component is clearly higher in binding energy (2p_{3/2} = 714 eV) and could therefore be attributed to the Fe³⁺ identified by Mössbauer spectroscopy. Moreover, etching studies confirmed the constant intensity of the Fe³⁺ signal, discarding its presence being due to surface oxidation. On the other hand, the high random variability of the LS/HS ratios on different scans hindered an accurate estimation of spin-state proportions via XPS.

CONCLUSIONS

The delamination/flocculation of a layered material in presence of a molecular Fe²⁺ complex has been employed here for the synthesis of a hybrid material in which superconductivity and SCO behavior are observed. Such functionalities had never before been successfully combined in a single material. Though superconductivity and SCO occur at complementary temperature regimes, the material is also a good electrical conductor at higher temperatures, namely above T_{SC}. This means that the material is a new example of the very few SCO conductors reported.^{16,17} In fact, preliminary results of conductivity measurements show an electrical conductivity as high as 0.93 S cm⁻¹ at room temperature on a free-standing highly oriented flake.

The organization of the SCO complexes in between TaS₂ and the ratio in which they are mixed are always restrained by the electroneutrality of the final structure. As a consequence, the Fe²⁺ centers are diluted within the TaS₂ layered lattice leading to a noncooperative gradual SCO transition.

The synthesis of this new chemically engineered hybrid material continues to extend the hybrid strategy that arises from the combination of molecule-based components with solid-state inorganic structures.^{3,4} Moreover, it also revisits the strategy of using TMDCs as a route for the combination of superconductivity with other interesting properties.³¹ Indeed, TaS₂ layers have been previously combined with both magnetic LDH layers and single-molecule magnets affording hybrid

magnetic superconductors with coexistence of superconductivity and ferromagnetism or single-molecule magnetism, respectively. The present material constitutes the third example of this class of hybrid superconductors in this case incorporating SCO magnetism.

In addition, a step further in the synthesis of TMDC hybrid materials is herein reported, consisting of the isolation of highly oriented plaquettes with anisotropic properties that mimic the behavior of the parent solid-state precursor compounds.

Finally, it is also suggested that the compound introduced here is potentially responsive to external stimuli such as an external applied magnetic field or light. In this line, subsequent investigation will be devoted to the study of the LIESST effect on this hybrid material as an approach to verify whether there is a synergy between superconductivity and SCO in the low temperature region. On the other hand, alternative studies will be devoted to the investigation of the prospective interaction between conductivity and SCO at the higher end of the temperature scale through the study of its magnetoresistive behavior.

ASSOCIATED CONTENT

Supporting Information

Electronic microscopy (SEM, TEM) characterization, XRPD diffractograms and Pawley refinements, additional magnetic characterization, and IR and XPS spectra. This material is available free of charge via the Internet at <http://pubs.acs.org>.

AUTHOR INFORMATION

Corresponding Author

*E-mail: eugenio.coronado@uv.es.

Notes

The authors declare no competing financial interest.

ACKNOWLEDGMENTS

Financial support from the EU (HINTS project and ERC Advanced Grant SPINMOL), the Spanish MINECO (Project Consolider-Ingenio in Molecular Nanoscience CDS2007-00010 and projects MAT2007-61584 and MAT2011-22785, cofinanced by FEDER), and the Generalitat Valenciana (Prometeo and ISIC Programs) is gratefully acknowledged. We also acknowledge J. M. Martínez for magnetic measurements and Helena Prima García for preliminary conductivity measurements.

REFERENCES

- (1) (a) Sanchez, C.; Belleville, P.; Popall, M.; Nicole, L. *Chem. Soc. Rev.* **2011**, *40*, 696. (b) Rocha, J.; Carlos, L. D.; Paz, F. A. A.; Ananias, D. *Chem. Soc. Rev.* **2011**, *40*, 926. (c) Chadov, S.; Qi, X.; Kübler, J.; Fecher, G. H.; Felser, C.; Zhang, S. C. *Nat. Mater.* **2012**, *9*, 541–545. (d) Cobley, C. M.; Chen, J.; Cho, E. C.; Wang, L. V.; Xia, Y. *Chem. Soc. Rev.* **2010**, *40*, 44.
- (2) (a) Day, P. *Molecules into Materials*; World Scientific: Singapore, 2007. (b) Coronado, E.; Galán-Mascarós, J. R.; Gómez-García, C. J.; Laukhin, V. *Nature* **2000**, *408*, 447–449. (c) Sato, O.; Iyoda, T.; Fujishima, A.; Hashimoto, K. *Science* **1996**, *272*, 704–705. (d) Coronado, E.; Giménez-López, M. C.; Korzeniak, T.; Levchenko, G.; Romero, F. M.; Segura, A.; García-Baonza, V.; Cezar, J. C.; de Groot, F. M. F.; Milner, A.; Paz-Pasternak, M. J. *Am. Chem. Soc.* **2008**, *130*, 15519–15532.
- (3) Clemente-León, M.; Coronado, E.; Forment-Aliaga, A.; Amorós, P.; Ramírez-Castellanos, J.; González-Calbet, J. M. *J. Mater. Chem.* **2003**, *13*, 3089–3095.

- (4) Coronado, E.; Martí-Gastaldo, C.; Navarro-Moratalla, E.; Ribera, A. *Inorg. Chem.* **2010**, *49*, 1313–1315.
- (5) Osada, M.; Sasaki, T. *J. Mater. Chem.* **2009**, *19*, 2503–2511.
- (6) Coleman, J. N.; Lotya, M.; O'Neill, A.; Bergin, S. D.; King, P. J.; Khan, U.; Young, K.; Gaucher, A.; De, S.; Smith, R. J.; Shvets, I. V.; Arora, S. K.; Stanton, G.; Kim, H.-Y.; Lee, K.; Kim, G. T.; Duesberg, G. S.; Hallam, T.; Boland, J. J.; Wang, J. J.; Donegan, J. F.; Grunlan, J. C.; Moriarty, G.; Shmeliov, A.; Nicholls, R. J.; Perkins, J. M.; Grievson, E. M.; Theuwissen, K.; McComb, D. W.; Nellist, P. D.; Nicolosi, V. *Science* **2011**, *331*, 568–571.
- (7) (a) Kaschak, D. M.; Lean, J. T.; Waraksa, C. C.; Saupé, G. B.; Usami, H.; Mallouk, T. E. *J. Am. Chem. Soc.* **1999**, *121*, 3435–3445. (b) Osada, M.; Ebina, Y.; Takada, K.; Sasaki, T. *Adv. Mater.* **2006**, *18*, 1023–1027.
- (8) Coronado, E.; Martí-Gastaldo, C.; Navarro-Moratalla, E.; Ribera, A.; Blundell, S. J.; Baker, P. J. *Nat. Chem.* **2010**, *2*, 1031–1036.
- (9) Coronado, E.; Martí-Gastaldo, C.; Navarro-Moratalla, E.; Burzurí, E.; Camón, A.; Luis, F. *Adv. Mater.* **2011**, *23*, 5021–5026.
- (10) (a) Cambi, L.; Szegő, L. *Ber. Dtsch. Chem. Ges.* **1931**, *64*, 167. (b) Cambi, L.; Malatesta, L. *Ber. Dtsch. Chem. Ges.* **1937**, *70*, 2067. (c) Schäfer, H. L.; Gliemann, G. *Einführung in die Ligandenfeldtheorie*; Akademische Verlagsgesellschaft: Frankfurt, 1967. (d) Sacconi, L. *Coord. Chem. Rev.* **1972**, *8*, 351.
- (11) (a) Real, J. A.; Andrés, E.; Muñoz, M. C.; Julve, M.; Granier, T.; Bousseksou, A.; Varret, F. *Science* **1995**, *268*, 265–267. (b) Létard, J.-F.; Guionneau, P.; Rabardel, L.; Howard, J. A. K.; Goeta, A. E.; Chasseau, D.; Kahn, O. *Inorg. Chem.* **1998**, *37*, 4432–4441. (c) Létard, J.-F.; Guionneau, P.; Nguyen, O.; Costa, J. S.; Marcén, S.; Chastanet, G.; Marchivie, M.; Goux-Capes, L. *Chem.—Eur. J.* **2005**, *11*, 4582–4589. (d) Bonhommeau, S.; Molnár, G.; Galet, A.; Zwick, A.; Real, J. A.; McGarvey, J. J.; Bousseksou, A. *Angew. Chem., Int. Ed.* **2005**, *44*, 4069–4073.
- (12) (a) Gaspar, A. B.; Ksenofontov, V.; Serebyuk, M.; Gütllich, P. *Coord. Chem. Rev.* **2005**, *249*, 2661–2676. (b) Niel, V.; Thompson, A. L.; Muñoz, M. C.; Galet, A.; Goeta, A. E.; Real, J. A. *Angew. Chem., Int. Ed.* **2003**, *42*, 3760–3763.
- (13) (a) Clemente-León, M.; Coronado, E.; López-Jordà, M.; Waerenborgh, J. C.; Desplanches, C.; Wang, H.; Létard, J.-F.; Hauser, A.; Tissot, A. *J. Am. Chem. Soc.* **2013**, *135*, 8655–8667. (b) Clemente-León, M.; Coronado, E.; López-Jordà, M.; Desplanches, C.; Asthana, S.; Wang, H.; Létard, J.-F. *Chem. Sci.* **2011**, *2*, 1121–1127. (c) Clemente-León, M.; Coronado, E.; López-Jordà, M. *Dalton Trans.* **2010**, *39*, 4903–4910.
- (14) (a) Akamatu, H.; Inokuchi, H.; Matsunaga, Y. *Nature* **1954**, *173*, 168. (b) Coronado, E.; Day, P. *Chem. Rev.* **2004**, *104*, 5419–5448.
- (15) (a) Williams, J. M.; Ferraro, J. R.; Thorn, R. J.; Carlson, K. D.; Geiser, U.; Wang, H. H.; Kini, A. M.; Whangbo, M. H. *Organic Superconductors. Synthesis, Structure, Properties and Theory*; Grimes, R. N., Ed.; Prentice Hall: Englewood Cliffs, NJ, 1992. (b) Ouahab, L. *Coord. Chem. Rev.* **1998**, *178–180*, 1501–1531. (c) Coronado, E.; Galan-Mascarós, J. R. *J. Mater. Chem.* **2005**, *15*, 66–74. (d) Coronado, E.; Giménez-Saiz, C.; Gómez-García, C. *Coord. Chem. Rev.* **2005**, *249*, 1776–1796.
- (16) (a) Takahashi, K.; Cui, H.-B.; Okano, Y.; Kobayashi, H.; Einaga, Y.; Sato, O. *Inorg. Chem.* **2006**, *45*, 5739–5741. (b) Faulmann, C.; Jacob, K.; Dorbes, S.; Lampert, S.; Malfant, I.; Doublet, M.-L.; Valade, L.; Real, J. A. *Inorg. Chem.* **2007**, *46*, 8548–8559. (c) Takahashi, K.; Cui, H.-B.; Okano, Y.; Kobayashi, H.; Mori, H.; Tajima, H.; Einaga, Y.; Sato, O. *J. Am. Chem. Soc.* **2008**, *130*, 6688–6689. (c) Nihei, M.; Takahashi, N.; Nishikawa, H.; Oshio, H. *Dalton Trans.* **2011**, *40*, 2154–2156.
- (17) (a) Djukic, B.; Lemaire, M. T. *Inorg. Chem.* **2009**, *48*, 10489–10491. (b) Djukic, B.; Seda, T.; Gorelsky, S. I.; Lough, A. J.; Lemaire, M. T. *Inorg. Chem.* **2011**, *50*, 7334–7343.
- (18) Radziszewski, B. *Ber. Dtsch. Chem. Ges.* **1882**, *15*, 2706–2708.
- (19) Chiswell, B.; Lions, F.; Morris, B. *Inorg. Chem.* **1964**, *1*, 110.
- (20) Pawley, G. S. *J. Appl. Crystallogr.* **1981**, *14*, 357.
- (21) Coelho, A. A. *TOPAS-Academic, Version 4.1, 2007*; see <http://www.topas-academic.net>.
- (22) Rodrigues, J. V.; Santos, I. C.; Gama, V.; Henriques, R. T.; Waerenborgh, J. C.; Duarte, M. T.; Almeida, M. J. *Chem. Soc., Dalton Trans.* **1994**, 2655.
- (23) Gamble, F. R.; DiSalvo, F.; Klemm, R.; Geballe, T. *Science* **1970**, *168*, 568–570.
- (24) Fang, L.; Wang, Y.; Zou, P.; Tang, L.; Xu, Z.; Chen, H.; Dong, C.; Shan, L.; Wen, H. *Phys. Rev. B* **2005**, *72*, 1–8.
- (25) Strict intercalation does not occur here, but rather only a slight doping of the dichalcogenide planes.
- (26) Nazar, L. F.; Jacobson, A. J. *J. Mater. Chem.* **1994**, *4*, 1419–1425.
- (27) Bistability refers to the ability of a system to be observed in two different electronic states in a certain range of some external perturbation (hysteretic system) from the following: Gütllich, P.; Goodwin, H. A. *Spin Crossover in Transition Metal Compounds*; Springer-Verlag: Berlin, 2004.
- (28) (a) Goodgame, D.; MacHado, A. *J. Chem. Soc., Chem. Commun.* **1969**, 1420–1421. (b) McGarvey, J. J.; Lawthers, I. *J. Chem. Soc., Chem. Commun.* **1982**, 906.
- (29) (a) Britto, S.; Thomas, G. S.; Kamath, P. V.; Kannan, S. *J. Phys. Chem. C* **2008**, *112* (25), 9510–9515. (b) Prasanna, S. V.; Kamath, P. V.; Shivakumara, C. *Mater. Res. Bull.* **2007**, *42* (6), 1028–1039. (c) Radha, A. V.; Kamath, P. V.; Shivakumara, C. *J. Phys. Chem. B* **2007**, *111* (13), 3411–3418.
- (30) (a) DiSalvo, F. J.; Schwall, R.; Geballe, T. H.; Gamble, F. R.; Osiecki, J. H. *Phys. Rev. Lett.* **1971**, *27*, 310–313. (b) Meyer, S. F.; Howard, R. E.; Stewart, G. R.; Acrivos, J. V.; Geballe, T. H. *J. Chem. Phys.* **1975**, *62*, 4411–4419. (c) Schlicht, A.; Schwenker, M.; Biberacher, W.; Lerf, A. *J. Phys. Chem. B* **2001**, *105*, 4867–4871.
- (31) Wong, H. V.; Evans, J. S. O.; Barlow, S.; Mason, S. J.; O'Hare, D. *Inorg. Chem.* **1994**, *33*, 5515.
- (32) Bruce, D. W.; O'Hare, D. *Inorganic Materials*; John Wiley & Sons: New York, 1997.
- (33) Meetsma, A.; Wiegers, G. A.; Haange, R. J.; de-Boer, J. L. *Acta Crystallogr.* **1990**, *C46*, 1598–1599.
- (34) Buchen, Th.; Gütllich, P.; Goodwin, H. A. *Inorg. Chem.* **1994**, *33*, 4573–4576.
- (35) Buchen, Th.; Gütllich, P.; Sugiyarto, K. H.; Goodwin, H. A. *Chem.—Eur. J.* **1996**, *2*, 1134.
- (36) Coronado, E.; Galán-Mascarós, J. R.; Giménez-López, M. C.; Almeida, M.; Waerenborgh, J. C. *Polyhedron* **2007**, *26*, 1838–1844.
- (37) Vijayalakshmi, R.; Yusuf, S. M.; Kulshreshtha, S. K. *J. Phys. Chem. Solids* **2004**, *65*, 975–979.
- (38) Gütllich, P.; Link, R.; Trautwein, A. *Inorganic Chemistry Concepts 3: Mossbauer Spectroscopy and Transition Metal Chemistry*; Springer-Verlag: Berlin, 1978.
- (39) (a) Tison, Y.; Martinez, H.; Baraille, I.; Loudet, M.; Gonbeau, D. *Surf. Sci.* **2004**, *563*, 83–98. (b) Peters, E. S.; Carmalt, C. J.; Parkin, I. P.; Tocher, D. A. *Eur. J. Inorg. Chem.* **2005**, 4179–4185.
- (40) NIST. *Chemistry WebBook, NIST Standard Reference Database Number 69*; Linstrom, P. J., Mallard, W. G., Eds.
- (41) Mazalov, L. N.; Asanov, I. P.; Varnek, V. A. *J. Electron Spectrosc. Relat. Phenom.* **1998**, 209–214.